IEEE Photonics Journal
An IEEE Photonics Society Publication

Open Access

Design of an Optical Trapping Device Based on an Ultra-High Q/V Resonant Structure

Volume 6, Number 6, December 2014

C. Ciminelli
D. Conteduca
F. Dell'Olio
M. N. Armenise

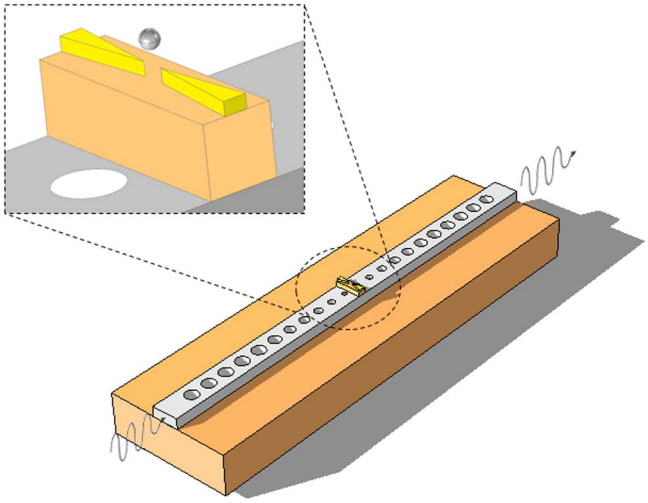

DOI: 10.1109/JPHOT.2014.2356496
1943-0655

IEEE photonics SOCIETY

IEEE

Design of an Optical Trapping Device Based on an Ultra-High Q/V Resonant Structure

C. Ciminelli, D. Conteduca, F. Dell'Olio, and M. N. Armenise

Optoelectronics Laboratory, Politecnico di Bari, 70125 Bari, Italy

DOI: 10.1109/JPHOT.2014.2356496

Manuscript received August 20, 2014; accepted August 27, 2014. Date of publication September 10, 2014; date of current version December 18, 2014. Corresponding author: C. Ciminelli (e-mail: c.ciminelli@poliba.it).

Abstract: A novel photonic/plasmonic cavity based on a 1-D photonic crystal cavity vertically coupled to a plasmonic gold structure is reported. The design has been optimized to achieve an ultra-high Q/V ratio, therefore improving the light–matter interaction and making the device suitable for optical trapping applications. Accurate 3-D finite element method (FEM) simulations have been carried out to evaluate the device behavior and performance. The device shows $Q = 2.8 \times 10^3$ and $V = 4 \times 10^{-4}(\lambda/n)^3$, which correspond to a $Q/V = 7 \times 10^6(\lambda/n)^{-3}$ with a resonance transmission around 50% at $\lambda_R = 1589.62$ nm. A strong gradient of the optical energy has been observed in the metal structure at the resonance, inducing a strong optical force and allowing a single particle trapping with a diameter less than 100 nm. The device turns out very useful for novel biomedical applications, such as proteomics and oncology.

Index Terms: Optical trapping, nanotweezer, photonic crystal cavity, plasmonic structure.

1. Introduction

Optical trapping has attracted strong interest in recent years, due to the ability to trap, detect, and manipulate small materials, such as living cells, single particles, and metal beads through optical signals. Many techniques have been proposed in literature, but the use of an optically based detection scheme provides high values of optical forces, so increasing the trapping efficiency and stability. At the same time, it also avoids a direct contact with the target object to trap, preventing its disruption or damage. In particular, integrated optical devices have demonstrated high values of the optical forces at low input power, making them suitable for quantum optics and medical, chemical, and biological applications. Due to their remarkable ability to confine the light at wavelength-scale and to enhance light–matter interaction, that are characteristics strongly requested in optical trapping applications, nanocavities have been received a notably attention by the scientific community. A key feature of such cavities is the quality factor (Q-factor) over the mode volume (V) ratio.

The research effort is focused on the enhancement of this figure of merit, improving the Q-factor and reducing the mode volume, which, in turn, corresponds to a decrease of the optical losses and a stronger photons confinement, respectively [1].

Since more than three decades, photonic crystals are the topic of an intense research effort motivated by the wide range of their applications and the new interesting physical effects that can be observed by exploiting them [2]–[4].

In particular, photonic crystals cavities have been largely investigated for several applications including telecom filters [5], [6] and biosensing [7]. These devices have shown high Q/V ratio both theoretically and experimentally. Q-factors up to Q = 10^9 and a Q/V ratio of the same order of magnitude have been theoretically obtained [8] in low mode volumes 1-D photonic crystal (PhCs) cavities. Experimental results have demonstrated a Q-factor up to 10^7 [9] and $Q/V = 3.2 \times 10^6(\lambda/n)^{-3}$ [10], with a mode volume less than the wavelength-scale.

PhC micro-cavities consisting of a single row of holes in a photonic wire [11]–[16] are an interesting alternative to 2-D PhCs cavities as they offer small mode volumes. *Q*-values exceeding 10^5 have already been experimentally demonstrated [16] by properly tapering the holes' size in order to reduce the mismatch between the waveguide mode and the evanescent Bloch mode in the photonic crystal structure. A systematic approach for designing such 1-D cavities has been reported in [17], where a resonator with $Q = 2 \times 10^6$ and $V = 0.38(\lambda/n)^3$, has been proposed. In Ref. [18], a Q-factor and a mode volume of the order of 10^5 and $10^{-3}(\lambda/n)^3$, respectively, have been achieved in a slotted nanobeam 1-D PhC cavity. An important figure of merit for such cavities is also the resonance transmission, that is requested to allow a good resolution for detection. Among the dielectric 1-D PhC micro-cavities featuring good transmission ($\geq$ 50%) at resonance, the best theoretical value of the Q/V ratio $(1.1 \times 10^6(\lambda/n)^{-3})$ has been obtained by the device reported in [19].

The high Q-factor makes PhC cavities suitable for devices such as low-threshold lasers, optical filters, as well as biosensors. However, the scaling of the dielectric nanocavities is diffraction limited, and this prevents a further decrease of their mode volume.

Plasmonic cavities, instead, do not suffer for this critical issue, and have provided smaller mode volumes, up to $V = 10^{-4}(\lambda/n)^3$ [20]. The confinement of the optical energy in such a small volume makes the plasmonic cavities suitable for many emerging applications, such as surface-enhanced spectroscopy, quantum cryptography, improvement of the radiative emission rate in silicon [21], and biosensing. Optical losses represent the most critical issue for such cavities, causing Q-factor values many orders of magnitude less than the ones obtained with dielectric PhC cavities. The balance between the two aspects of strong light confinement and high optical losses leads to not so high Q/V ratios, with a state of the art record of $10^5(\lambda/n)^{-3}$ [22].

Hybrid cavities based on a dielectric PhC micro-cavity coupled to a metal surface have already been proposed [23], [24], allowing to overcome the diffraction limited scaling of the mode volume and providing, at the same time, strong both spatial and spectral energy densities. The state-of-the-art value of the Q/V ratio in a hybrid configuration is $8 \times 10^4(\lambda/n)^{-3}$ [24]. This value is much lower than that in dielectric cavities. The most evident advantage of such hybrid devices is a high-energy confinement in the medium with a lower refractive index. A strong enhancement of the light–matter interaction makes them suitable for biosensing applications, such as optical trapping [25]–[27].

We propose a novel hybrid resonant device based on a 1-D PhC micro-cavity vertically coupled to a gold structure, improving the state-of-the-art of hybrid micro-cavities more than two orders of magnitude in terms of Q/V figure of merit.

The obtained Q/V value is six times higher than that of 1-D PhC cavities with a resonance transmission of about 50%. The main advantage of the proposed hybrid cavity is the strong confinement of the electromagnetic field in the metal structure in resonant condition, with a sharp gradient of the optical energy at the metal tips. This allows obtaining high values of the optical forces close to the metal region, making the device able to trap single nanoparticle, with a diameter less than 100 nm. The strong optical energy gradient allows also the device to work with low input optical power, less than 1 mW, so decreasing the effect of thermal heating in the surrounding fluid and then the effects of Brownian motion of particles to trap [28], [29]. A high probability for trapping a nanoparticle close to the metal is confirmed by the strong stiffness and the high stability of the optical traps. It makes the device suitable for several emerging applications, such as proteomics and genetics.

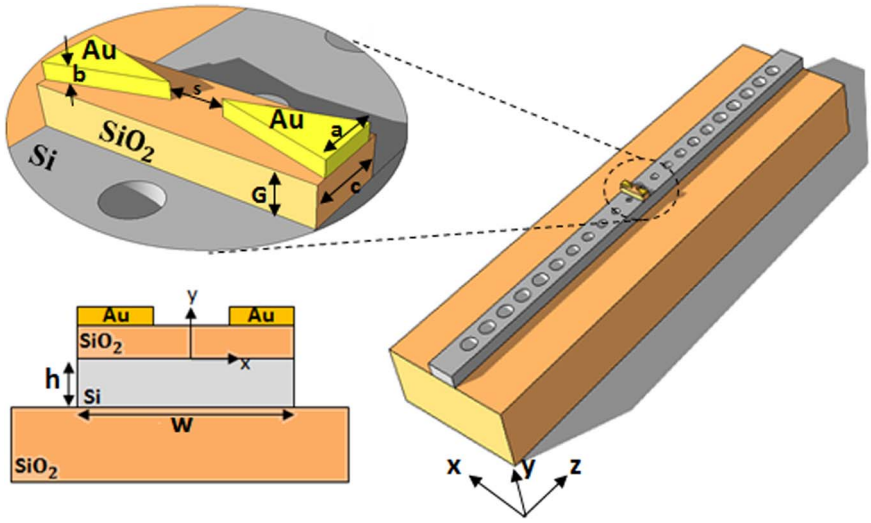

Fig. 1. Hybrid device configuration and its cross-section. The inset highlights the metal structure with a triangular shape.

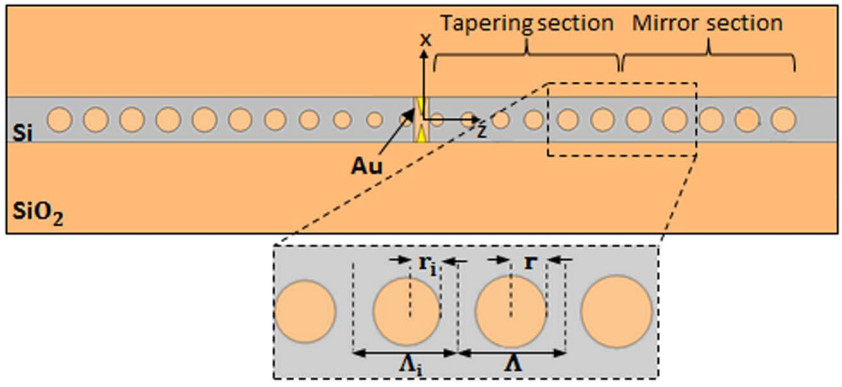

Fig. 2. Top view of the hybrid device, with a focus on the PhC configuration in the inset.

2. Device Configuration

The device structure includes a 1-D PhC dielectric micro-cavity embedded in a silicon (Si) photonic wire, which is coupled to a plasmonic structure, as in Fig. 1. The inset is a magnification of the gold structure, highlighting also the thin layer of silicon dioxide placed between the silicon wire and the metal strip. The wire has a width of $w = 490$ nm and a thickness $h = 220$ nm. The thickness of the buried oxide is 1 μm.

The dielectric cavity is made by two mirror sections, each consisting of five holes with uniform radius r and period Λ, and two tapered regions, in which the hole radii and the periods are not uniform (they are denoted as r_i and Λ_i, respectively, with $i = 1, 2, \ldots, 6$), as it is shown in Fig. 2. Each tapered section includes six holes. The resonant behavior is induced by the presence of the tapered sections, as the structure does not include any other defect. The medium surrounding the cavity is assumed to be water, to consider the real situation of nanoparticles flowing in a fluid.

We have chosen this PhC cavity geometry because it allows for a small mode volume and low optical losses [8]. The radius of the air holes gradually increases from the middle of the cavity to the mirror section [16].

A plasmonic structure is vertically coupled to the dielectric cavity so further minimizing the volume of the resonating mode.

We have chosen a triangular geometry that is typical of a *bowtie* nanoantenna [30] for the metal structure, with a thin layer in water between two triangular strips in Au. The gap between the metal layer and the wire is denoted with *G*, and the distance between the metal tips with *s*. We assume that the thickness *b* and the side length along *z*-axis *a* of the gold layer are equal to 30 nm and 50 nm, respectively. The metal structure, which is denoted as *bowtie*, is supported by a SiO_2 layer having a length $c = 110$ nm and a thickness *G*. We assume $y = 0$ at the Si-wire/oxide interface, $z = 0$ at the center of the *bowtie*, and $x = 0$ at the center of the silicon wire.

The *bowtie* acts as a funnel for the light propagating in the PhC cavity and a vertical coupling with the metal structure is achieved at the resonance, providing a strong confinement of the optical energy around the gold tips. The vertical light coupling of the Bloch mode propagating in the PhC to the *bowtie* is due to the strong dielectric discontinuity between metal and dielectric layers, achieving a strong subwavelength confinement of the optical energy at the metal tips when two gold layers are close to each other, overcoming the diffraction limit typical in dielectric structures and achieving a strong enhancement of the field.

The light is trapped in the *bowtie* from the silicon nanowire, unlike a typical configuration of a nanoantenna where the field used for excitation of localized surface plasmon polariton (SPP) is an incident plane wave.

A typical conductor-gap-silicon (CGS) structure in the vertical direction has been realized. However, the novelty of the proposed design is related to the presence of the *bowtie* structure, in place of a metal layer as in a typical CGS configuration, preventing the propagation of SPP modes, but providing the strong localization of the optical energy close to the *bowtie* tips.

A great advantage of our new configuration is relevant to the presence of a PhC in the nanowire. In fact, PhC works as a mirror at a wavelength inside the photonic bandgap; therefore, the light is almost totally reflected by the mirror holes, preventing its confinement in the cavity. At the resonance, a tight confinement in the cavity between the inner holes in a volume at nanoscale and a strong amplification of the optical field are achieved, allowing an efficient interaction between the PhC and the *bowtie*.

The physical phenomena observed in the photonic/plasmonic cavity provide a small mode volume, comparable to the state-of-the-art of plasmonic cavities, and also a high Q-factor, due to the presence of the PhC dielectric cavity in the vertical coupling structure. The Q-factor is lower than the typical values obtained by the cavity without the bowtie, but more than one order of magnitude greater than those achieved by typical plasmonic nanoantennas. Similar performance corresponds to an improvement of Q/V ratio of the state-of-the-art of hybrid cavities.

3. Design and Numerical Results

The proposed device has been designed with the aim of maximizing the Q/V ratio, as well as keeping high the resonance transmission $T \geq 50\%$. An ultra-high Q/V ratio, which could imply a very strong light–matter interaction in the resonator, is demanded by several applications such as single-photon sources, biosensors and nonlinear optical devices, while the condition of $T \geq 50\%$ allows good resolution detection.

We have chosen the radii and the periods of both the tapered (r_i, Λ_i) and the mirror sections (r, Λ), to obtain a high Q-factor, optimizing the confinement of the optical energy between the central holes and improving the coupling with the metal bowtie in resonance conditions.

The radius and the period of the mirror holes have been chosen equal to 130 nm and 390 nm, respectively [31]. The holes' radii in the tapered section strongly influence both the resonance transmission and the Q-factor. Large radius of the smallest hole, i.e., $R_1 = 80$ nm, provide a high resonance transmission, but a decrease of the Q-factor as well. Otherwise, a smaller value, i.e., $R_1 = 50$ nm, provides an opposite cavity behavior, with a higher Q-factor and a less evident resonance condition. The value of $R_1 = 70$ nm has been assumed as the best compromise between these two figures of merit for the 1-D PhC dielectric cavity. Also, the other radii

and the periods (r_i, Λ_i) of the tapered section have been optimized to satisfy those requirements. We have considered different tapering configurations to evaluate the device performance. The parameter considered for the optimization of the tapered section is the filling fraction, defined as $FF = \pi \cdot r_i^2/w \cdot \Lambda_i$. The period of the holes has been decreased linearly from the mirror $(\Lambda = 390\ nm)$ to the smallest hole, for which it has been fixed at $\Lambda_1 = 330$ nm to obtain a resonance wavelength around 1590 nm. A linear increase of the filling fraction from the center to the mirror, which corresponds to a quadratic increase of the radii holes, has demonstrated to provide the best performance of the 1-D PhC dielectric cavity, in terms of Q-factor and resonance transmission, because it improves the matching between the fundamental mode of the photonic wire and the evanescent Bloch mode in the PhC.

We have used a 3-D FEM approach to simulate the behavior of the device, assuming that the cavity was excited by a fundamental TE polarized beam. The wavelength has been swept in a wide range from 1500 nm to 1650 nm in order to evaluate the device spectral response. The dispersion of the Si and SiO_2 refractive indices has been included via the Sellmeier model [32], assuming $n_{Si} = 3.472$ and $n_{SiO2} = 1.444$ at $\lambda = 1590$ nm. In order to simulate the absorption in the surrounding medium, the refractive index of water has been assumed to be complex with a real part $n_{H20} = 1.318$ and an imaginary part $k = 1.03 \times 10^{-4}$ at $\lambda = 1590$ nm [33].

The mode volume has been evaluated by using the following equation [34]:

$$\frac{\iiint_V \varepsilon |E|^2 dV}{\max\left[\varepsilon |E|^2\right]} \tag{1}$$

where ε is the relative permittivity, $|E|^2$ is the squared module of the electric field, and V is the whole calculation volume.

We have obtained $Q = 4.1 \times 10^3$, $V = 0.6(\lambda/n)^3$, where λ is the resonance wavelength and n the refractive index of the silicon, corresponding to a $Q/V = 6.8 \times 10^3(\lambda/n)^{-3}$, through 3-D FEM simulations of the PhC dielectric cavity without the presence of the metal *bowtie*. The resonance transmission has been evaluated by the ratio between the outflow power integrated over the output cross-section and the power inflow at the input boundaries $(P_{in} = 10\ mW)$, obtaining a high value up to $T = 92\%$ at $\lambda_R = 1590$ nm.

The PhC dielectric cavity has been optimized mainly to reduce optical losses and to obtain a strong confinement of the optical energy between the central holes, so improving the vertical coupling between the PhC and the *bowtie* at resonance, when the metal is deposited above the PhC, defining the configuration of the hybrid cavity.

After the design of the PhC dielectric cavity, two gold strips with a triangular shape have been placed between the inner holes, as described above. This configuration of a typical *bowtie* antenna for the metal structure has been considered due to its higher sensitivity [35]. The parameters *b* and *a* of the metal strips have been kept constant to 30 nm and 50 nm, respectively, as shown in Fig. 1.

In order to take the dispersion of the Au complex permittivity (ε_{Au}) into account, we have used the Lorentz-Drude model [36]. Thus, for each value of the wavelength we considered the corresponding value of ε_{Au}. At $\lambda = 1590$ nm, we have assumed $\varepsilon_{Au} = (-97.9745 + 11.6790i)$. As already mentioned, the spectral response of the hybrid photonic/plasmonic micro-cavity has been obtained by hundreds of simulations for λ varying in a wide range. In each simulation we have launched at the device input a CW beam and have observed the output power. This simulation technique intrinsically takes into account the dispersion of ε_{Au}.

A parametric analysis on both parameters *s* and *G* has been carried out to evaluate the best configuration of the hybrid device. We have considered the gap *G* ranging from 50 nm to 200 nm, assuming an initial value of $s = 50$ nm.

The increase of *G* improves the resonance transmission and the Q-factor because the larger distance of the metal structure from the dielectric wire reduces the optical losses. Unfortunately, a larger *G* value also implies a decrease of the *bowtie*/wire coupling efficiency, thus reducing

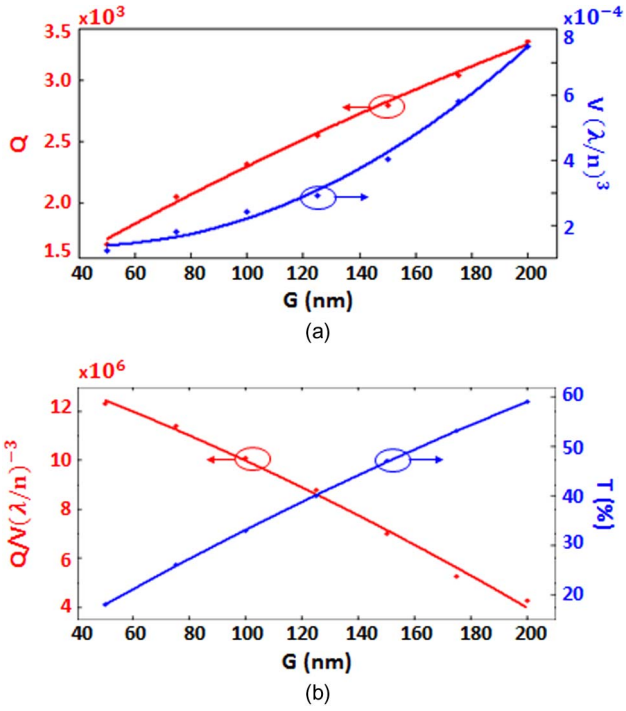

Fig. 3. (a) Quality factor (red curve) and mode volume (blue curve) and (b) Q/V ratio (red curve) and resonance transmission (blue curve) of the hybrid device as a function of the gap *G* with a *bowtie* width *s* of 50 nm.

the light confinement by the *bowtie* and increasing the mode volume. We have achieved a good compromise for $G = 150$ nm, which corresponds to a resonance transmission around $T = 50\%$, as shown in Fig. 3.

In Fig. 4, a second parameter analysis has been carried out on the slot width*s*, from 25 nm to 150 nm, keeping constant the gap $G = 150$ nm.

The best tradeoff between T and Q/V was achieved for $G = 150$ nm and $s = 50$ nm. In fact, even if an increase of s provides higher transmission values and Q-factors, an increase of the mode volume has been also observed, which causes a strong decrease of the optical energy between the metal tips.

The optimized configuration ($s = 50$ nm and $G = 150$ nm) provides $Q = 2.8 \times 10^3$ and $V = 4 \times 10^{-4}\ (\lambda/n)^3$, which corresponds to a $Q/V = 7 \times 10^6\ (\lambda/n)^{-3}$ with a resonance transmission of $T = 47\%$, as shown in Fig. 5. As clearly shown in Fig. 5, the cavity supports just one resonant mode. Therefore, the input beam can excite only that mode.

From the comparison of the PhC dielectric cavity performance with the photonic/plasmonic one, preserving the same PhC configuration and adding the *bowtie* structure, we have observed a slight decrease of Q-factor from 4.1×10^3 to 2.8×10^3, but a strong improvement of V. The improvement is around three order of magnitude, exactly from $V = 0.6\ (\lambda/n)^3$ with the dielectric cavity to $V = 4 \times 10^{-4}\ (\lambda/n)^3$. Those results confirm an optimization of the Q/V ratio of three orders of magnitudes, from $Q/V = 6.8 \times 10^3 (\lambda/n)^{-3}$ with the dielectric configuration to $Q/V = 7 \times 10^6\ (\lambda/n)^{-3}$ with the hybrid cavity, demonstrating the performance improvement relating to the photonic/plasmonic cavity, as shown in Table 1, and justifying the use of the bowtie to provide a higher spatial energy density.

An increase of two orders of magnitude for the figure of merit Q/V achieved with the cavity proposed has been observed when compared to the performance achieved by other hybrid devices based on a photonic crystal structure [24].

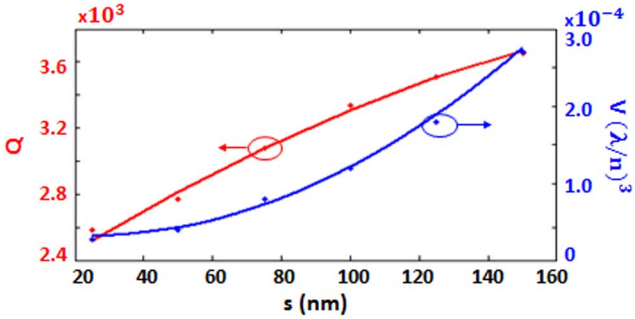

(a)

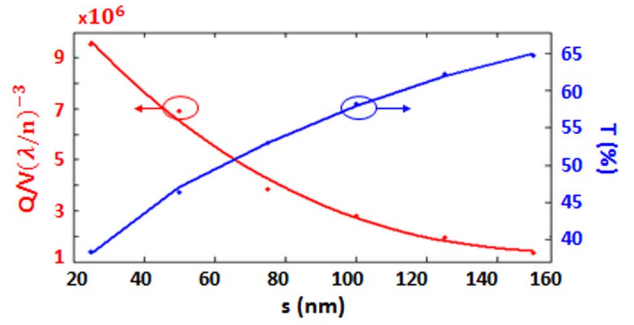

(b)

Fig. 4. (a) Quality factor (red curve) and mode volume (blue curve) and (b) Q/V ratio (red curve) and resonance transmission (blue curve) of the hybrid device as a function of the *bowtie* width *s* with a gap $G = 150$ nm.

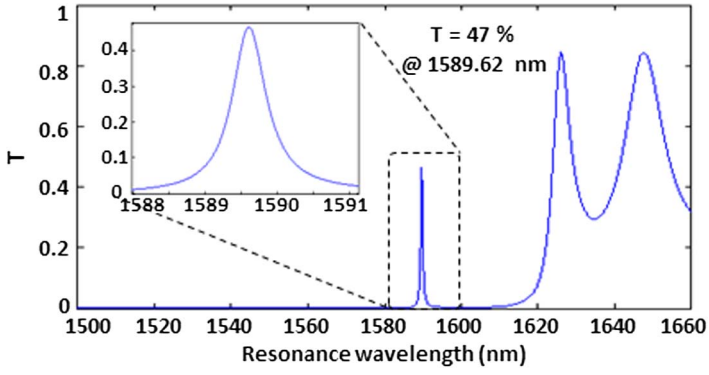

Fig. 5. Transmission spectrum of the hybrid device with $s = 50$ nm and $G = 150$ nm. The inset highlights the spectrum in wavelength range 1588 nm–1591 nm with a resonance transmission T $= 47\%$ and Q $= 2.8 \times 10^3$ at $\lambda = 1589.62$ nm.

The modal distribution in the metal structure and in the silica layer at z $= 0$ has been reported in Fig. 6, with a magnification of the region around the gold tips.

The influence of the gold structure on the device performance can be observed by the modal distribution in the *bowtie* (see Fig. 6) at the resonance and by the behavior of the mode volume versus s (see Fig. 4), demonstrating a decrease of about one order of magnitude of V with s varying from 150 nm to 25 nm.

A high confinement of the electric field lines around the gold structure at resonance, shown in Fig. 6, confirms a strong-light matter interaction inside the metal strips.

The values of the optical energy evaluated in the PhC cavity in presence of the metal structure are typically two orders of magnitude less than the value achieved in the PhC without the

TABLE 1

Comparison of the performance obtained with the PhC dielectric cavity and the photonic/plasmonic one, adding the bowtie nanoantenna

	Q	V $(\lambda/n)^3$	Q/V $(\lambda/n)^{-3}$	T (%)
Dielectric PhC cavity	4.1×10^3	6×10^{-1}	6.8×10^3	92
Photonic/plasmonic cavity	2.8×10^3	4×10^{-4}	7.0×10^6	47

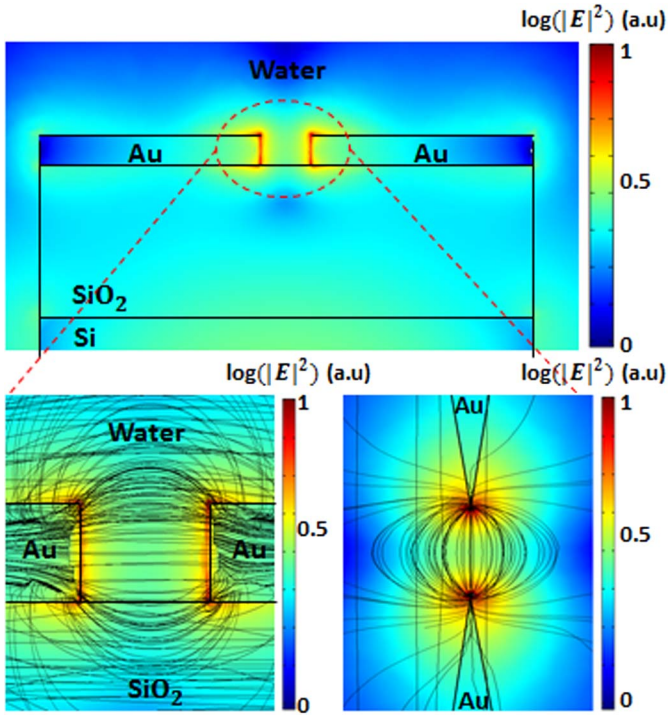

Fig. 6. Modal distribution in the hybrid device at resonance (1589.62 nm) with $s = 50$ nm and $G = 150$ nm in $z = 0$. Logarithmic scale of $|E|^2$ and electric field mapping have been reported with a focus on the metal *bowtie* in the insets.

bowtie, due to the amount of energy vertically coupled from the PhC to the gold structure and for the metal absorption. Furthermore, the strong confinement of the optical energy around the metal tips provides energy values even more three orders of magnitude greater than those evaluated in the PhC of the hybrid cavity, as shown in Fig. 7, where the $|E|^2$ distribution of at the surface of the *bowtie* nanoantenna and in the PhC cavity is shown. To further investigate the confinement of the E-field at the *bowtie* tips, the spatial distribution of the electromagnetic energy density has been calculated (see Fig. 8). The energy density, similarly to the E-field, exhibits very strong discontinuities at the tips of the *bowtie* structure.

The strong confinement of the optical energy at the metal tips makes the cavity very sensitive to the pattern of the *bowtie*, and particularly to the sharpness of the tips. The cavity performance has been also evaluated for several values of the radius of the tip until 10 nm. A slight decrease of Q-factor and resonance transmission has been observed, and particularly a strong increase of the mode volume has been achieved increasing the radius, corresponding to a decrease of Q/V ratio. A $Q/V \geq 10^6\ (\lambda/n)^{-3}$ has been evaluated with a radius of the rounder tip less than 10 nm, obtaining $Q/V = 3.3 \cdot 10^6\ (\lambda/n)^{-3}$ and $Q/V = 1.5 \cdot 10^6\ (\lambda/n)^{-3}$ with a radius of 5 nm and 10 nm, respectively. A similar behavior confirms a performance better than the state-of-the-art with a more realistic configuration of the bowtie structure.

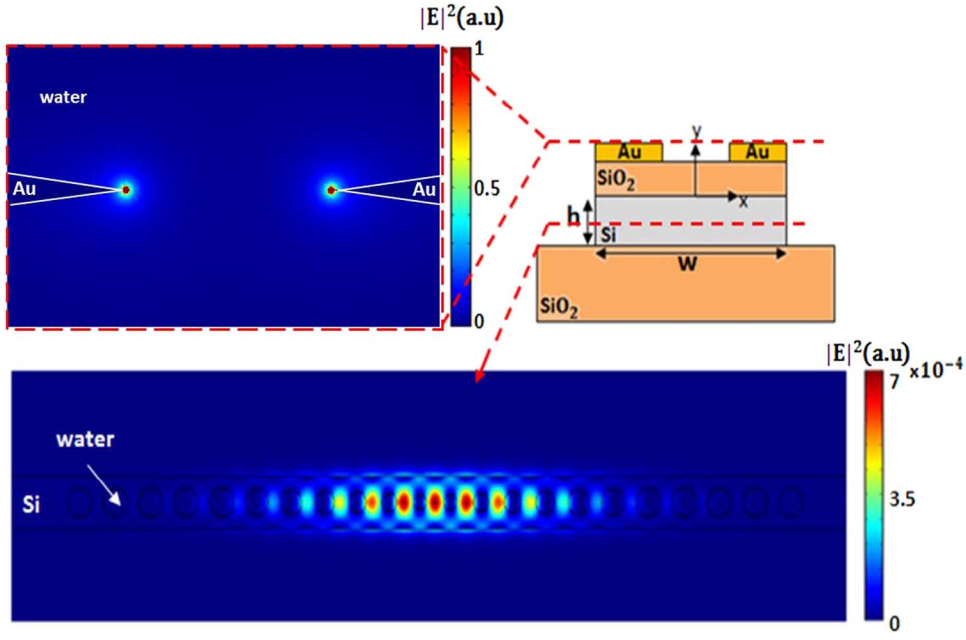

Fig. 7. Distribution of $|E|^2$ at the surface of the *bowtie* nanoantenna (in the inset) and in the PhC cavity of the hybrid device.

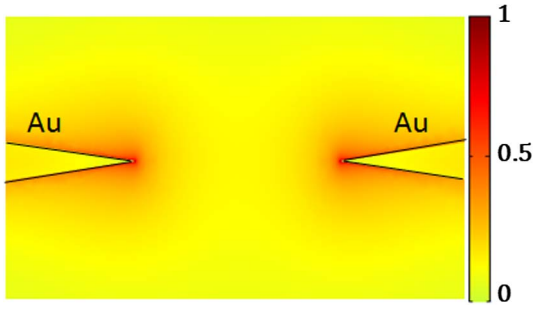

Fig. 8. Distribution of the normalized energy density at the surface of the *bowtie* nanoantenna (in log scale).

Even if high values of the optical energy have been calculated at the metal tips under resonance condition, as a typical behavior in a plasmonic slotted structure, only 1% of the total energy is confined in the ultra-small volume of the metal *bowtie*, while the most is in the Si-wire (approximately 90%).

An increase of the light confined in the cavity at the resonance could be achieved by decreasing the thickness of the silica layer and the slot width, but this optimization step also provides a lower resonance transmission and, particularly, a strong decrease of the Q-factor, reducing the detection resolution and the spectral energy density.

A similar behavior makes the hybrid device suitable for optical trapping, due to an ultra-high gradient of the electromagnetic field in the plasmonic structure, providing strong optical forces for trapping nanoparticles [37].

4. Design of a Nanotweezer for Optical Trapping

In the last few years, there is a continuous and increasing interest in optically based detection and manipulation techniques. The use of an optical beam provides high efficiency in trapping at

lower values of the input power. This peculiarity makes the optical tweezers particularly suitable for several medical, chemical and biological applications [38]–[40]. Due to the high values of the optical forces applied in a safety condition for living cells, recent studies have demonstrated the ability for the recognition and the analysis of viruses and single DNA sections with a size up to 5 nm, not easily granted by different techniques. The optical trapping is also useful to control non biological targets in quantum optics, such as metal particles, for the colloidal dynamics and the particle sorting [41], [42].

The traditional free space optical trapping techniques are affected by the diffraction limit, that prevents the control of particles at nanoscale. Furthermore, the use of the bulk optics, with lenses for focusing a laser beam, exerts optical forces large enough to trap particles with micrometer size. The trapping of smaller particles is very difficult because the trapping force is inversely proportional to the 3rd power of radius [42]. This limit has been overcome by the use of integrated optical devices.

The optical force can be expressed as [42]

$$\mathbf{F} = \oint_{S} (\mathbf{T}_M \times \mathbf{n}) dS \tag{2}$$

where $\mathbf{T}_M$ is the Maxwell stress tensor, S is the particle surface, and $\mathbf{n}$ is the outgoing vector normal to the surface. For a particle with a diameter smaller than 100 nm the optical force can be also expressed as the force gradient for a Rayleigh particle [43]

$$F_{grad} = \left(n_m^2 r^3/2\right)\left[(m^2-1)/(m^2+2)\right]\nabla|E|^2 \tag{3}$$

where n_m is the refractive index of the medium, m is the ratio of the particle refractive index to the refractive index of the medium, and E is the electric field. From (3) it is evident the influence of the gradient of the optical energy on the optical force applied to the particle.

Recently, several configurations have been proposed providing high values of the optical energy and, then, strong optical forces, such as slot waveguides, whispering gallery mode (WGM) resonators and, particularly, plasmonic and PhC cavities [44]. The latter are able to guarantee high values of the optical forces, together with a good stability of the optical trapping. The highest values of the optical energy gradient, have been demonstrated in plasmonic devices. However, plasmonic cavities are affected by the thermophoresis [45]. An increase of the optical energy corresponds to a thermal heating, that causes a repulsion of particles away from the warmest regions. This effect appears for values of the optical input even of the order of 10 mW.

A similar behavior makes the trapping more difficult. A disruption or a damage of the biological particles can be also observed for a strong temperature increase. These physical effects can be avoided with lower optical input power, even if this corresponds to a decrease of the optical forces.

The 1-D PhC cavity in the proposed hybrid device has been designed with the aim to improve the coupling with the metal structure, and then to get high optical energy peaks at the metal tips. Strong optical forces are expected also with low input optical power, overcoming the critical issue of the thermophoresis related to the use of a plasmonic configuration.

The efficiency of the hybrid device for the optical trapping has been evaluated by 3-D FEM simulations.

The trapping force has been computed considering a spherical polystyrene bead ($n = 1.57$ at $\lambda = 1590$ nm) in a volume of space close to the metal structure (see Fig. 9). We have chosen a particle in polystyrene, because the refractive index $n = 1.57$ is very similar to the refractive index of living cells or proteins, that are usually in experimental works the target for the optical trapping. As expressed in (3), the force gradient is also influenced by the ratio m. A ratio of $n_{polys}/n_{water} = 1.2$ has been already experimentally demonstrated to provide a stable optical trap [46].

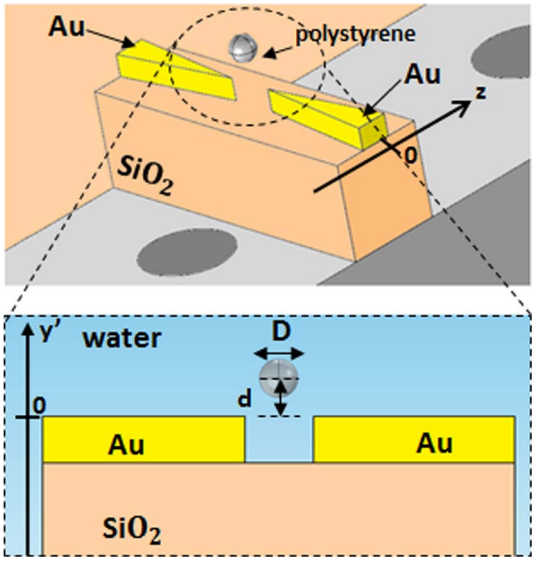

Fig. 9. Hybrid device configuration for the optical trapping of a polystyrene nanoparticle.

The optical force on the particle has been calculated by integrating $\mathbf{T}_M$ on a surface with a radius 5 nm larger than the particle radius.

An accurate evaluation of optical forces has been provided positioning the boundary layers of the computational domain sufficiently far away from the particle and other scattering objects, avoiding that the undesired reflection of the fields from the boundary of the computational domain could affect the evaluation of optical forces. A very fine mesh (with a minimum element of 2 nm) and long computational time have been requested to evaluate the optical force with high accuracy.

The particle has been assumed inside the gap between the metal tips. This position corresponds to a stronger confinement of the optical energy, due to the coupling with the 1-D PhC cavity, and then to a stronger optical force exerted on a particle, with respect to other potential optical traps, such as at any metal tip. The optical trap inside the *bowtie* provides a more efficient control over the particle position for its detection and manipulation.

The hybrid device performance, in terms of optical trapping, are similar to those obtained by a typical nanoantenna for a particle with a diameter bigger than the *bowtie* width [37].

The main advantage of the proposed hybrid device is related to the smaller diameter $(D \leq s)$ of the particles able to be trapped inside the metal structure.

We have evaluated the optical force on a polystyrene particle with $D = 40$ nm in different positions along y′-axis and *z*-axis. The optical force along *x*-axis has been neglected, due to the physical confinement of the metal strips, that prevents any movement of the particle. We have considered y′-axis (see Fig. 9) different from *y*-axis represented in Fig. 1, to simplify the study of optical forces versus particle displacement along this direction. The position $y' = 0$ corresponds to the case of the particle center at the upper surface of the metal structure, where a maximum gradient has been obtained, and $z = 0$ is in the plane of the metal tips, as shown in Fig. 9.

The input power has been assumed equal to 10 mW and the optical force has been evaluated for different values of the particle position along both directions. We have defined d as the distance of the particle from the upper surface of the metal slot along y′-axis, and p as the particle displacement from the metal tips along *z*-axis.

Assuming the particle centered on the metal *bowtie*, d has been varied from -5 nm to $+120$ nm along the y′-axis, where the particle is not affected by the trapping force, and from -100 nm to $+100$ nm along *z*-axis.

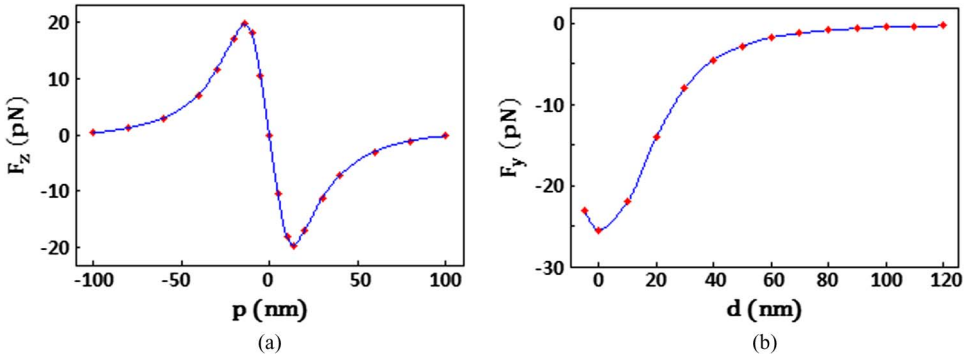

Fig. 10. Optical force for different values of p along *z*-axis (a) and of d along y′-axis (b) for a particle of D = 40 nm and P_{in} = 10 mW.

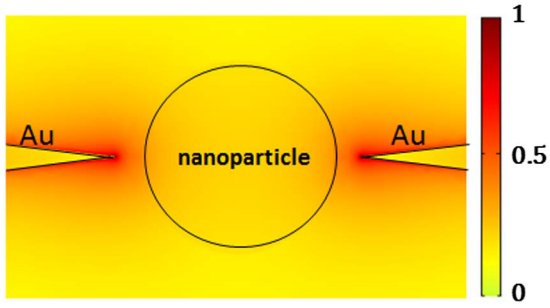

Fig 11. Distribution of the normalized energy density at the surface of the *bowtie* nanoantenna when a nanoparticle is close to it, i.e., d = 0 (in log scale).

The optical force values along both axis have been reported in Fig. 10.

A maximum value of the optical force up to $F = -26$ pN has been evaluated at $y' = 0$. A value of $d > 120$ nm along the y′-axis is considered a free position for the polystyrene particle. The maximum value of F_z is ± 20 pN evaluated at $d = \pm 15$ nm. A symmetry of F_z around $d = 0$ has been obtained, with $F_z = 0$ at $z = 0$, confirming the absence of a net force on the particle in this position, defined as the equilibrium point. It means that if a particle is flowing in a region close to the metal slot, where the optical forces are not negligible, it is affected by an attractive force that brings the particle around its equilibrium point, keeping it in that stable position. A similar behavior has been obtained disregarding repulsion forces, such as thermal and drag forces, due to the thermophoresis effect and the fluid velocity, respectively, that cause a standard deviation on the particle's position around its equilibrium point.

The confinement of the electromagnetic field within the region occupied by the nanoparticle depends on its position and it is always much lower than 1%. We have calculated also the spatial distribution of the electromagnetic energy density at the bowtie surface when the nanoparticle is close to the hybrid device $(d = 0)$. By comparing the result of that evaluation (see Fig. 11) and the energy density distribution when no particle is close to the micro-cavity (see Fig. 8), we can conclude that the nanoparticle influences the energy density distribution, even if the energy density keeps confined very close to the Au/water discontinuity also when the nanoparticle is close to the *bowtie*.

From the force calculation, other two important figures of merit for the evaluation of the optical trapping can be extracted: the stability and stiffness.

The trapping stiffness is defined as [47]

$$K = \frac{\partial F}{\partial X}\Big|_{\text{equilibrium}} \tag{4}$$

TABLE 2

Performance of the hybrid cavity for optical trapping as a function of G with $s = 50$ nm

G (nm)	Q	V $(\lambda/n)^3$	Q/V $(\lambda/n)^{-3}$	T (%)	F (pN)
50	1.66×10^3	1.6×10^{-4}	1×10^7	17	-35
100	2.32×10^3	2.5×10^{-4}	9×10^6	31	-31
150	2.80×10^3	4.0×10^{-4}	7×10^6	47	-26

where F is the optical force, and ∂X is the particle displacement along the y′-axis or z-axis. A high stiffness corresponds to a stable position around the equilibrium point for the trapped particle. A trapping stiffness $K = 80$ pN/nm $\cdot$ W has been obtained, around one order of magnitude higher than typical PhC dielectric cavities [48] and higher also than simple nanoantennas [37] for trapped particles with $D < 50$ nm. A stronger stiffness of 150 pN/nm $\cdot$ W has been evaluated along the z-axis.

The other figure of merit is the stability S of the optical trap. Many factors make the trapping and its stability difficult, such as the drag force of the fluid and, particularly, the thermal heating. The thermal force is repulsive and opposite to the attraction effect of the optical force. An optical force larger than the thermal one is requested to obtain a stable trap. The stability is defined as [49]

$$S = \frac{U}{K_B T} \tag{5}$$

where U is the work necessary to carry the particle from a free position $(F = 0)$ to the equilibrium point, K_B is the Boltzmann's constant, and T the operative temperature.

We have supposed that the hybrid device works at room temperature $(T = 300\ K)$. A strong confinement of the optical energy causes a temperature increase, with an undesired thermophoresis effect. A trap can be assumed to be stable if $S \geq 10$.

The particle size and the input power are the parameters that mostly influence the stability. An increase of the Brownian motion of small size particles $(D < 100$ nm$)$ can make the trap more unstable, while higher values of the input power amplify the thermal heating. Both effects cause a decrease of the stability factor S.

We have calculated the stability for the hybrid device with an input power of 10 mW and a particle diameter $D = 40$ nm, by integrating the work requested to carry the particle from $y' = 0$ to $y' = 120$ nm. From the computation of the optical force reported in Fig. 10, we have obtained $S = 210$, demonstrating a high stability for the trapping of a nanoparticle in the hybrid device, corresponding to long trapping time [28].

Experimental works have demonstrated a temperature change of 3 K for an input power of 10 mW [46]. A similar local temperature increase leads to bubble formation in the fluid, moving away the particles that are flowing in that region. A decrease of the input power is needed to reduce the thermophoresis effect. We have also demonstrated a stability $S \geq 10$ with an input power less than 1 mW, which is a typical power value already used in many experimental works with plasmonic configurations, such as the *bowtie* nanoantenna discussed in [42]. The performance obtained by the simulations confirm that the hybrid device is suitable for the optical trapping of nanoparticles $(D < 100$ nm$)$ with a high stability and consequent long detection time.

We have analyzed the performance of the hybrid cavity for optical trapping, for several values of G and s to define the relationship between Q/V and optical forces, stability and stiffness. A slight increase of optical forces and stability has been observed decreasing G, due to an increase of the Q/V ratio. We have obtained $F = -31$ pN with $G = 100$ nm and $s = 50$ nm and $F = -35$ pN with $G = 50$ nm and $s = 50$ nm, corresponding to a $Q/V = 9 \times 10^6\ (\lambda/n)^{-3}$ and $Q/V = 1 \times 10^7\ (\lambda/n)^{-3}$. However, a strong decrease of the resonance transmission has been observed decreasing G, obtaining $T = 31\%$ and $T = 17\%$ with $G = 100$ nm and $G = 50$ nm, respectively, as shown in Table 2.

TABLE 3

Performance of the photonic/plasmonic cavity with an increasing radius of the rounded metal tips of the bowtie nanoantenna with $P_{in} = 10$ mW

Radius (nm)	Q	V $(\lambda/n)^3$	Q/V $(\lambda/n)^{-3}$	T (%)	F (pN)	S
0	$2.80\text{x}10^3$	$4\text{x}10^{-4}$	$7\text{x}10^6$	47	-26	210
5	$2.65\text{x}10^3$	$8\text{x}10^{-4}$	$3.3\text{x}10^6$	44	-6	60
10	$2.35\text{x}10^3$	$1.5\text{x}10^{-3}$	$1.5\text{x}10^6$	41	-4	40

Assuming $G \leq 100$ nm, a decrease of the resonance transmission around 10% has been obtained with a radius of 10 nm of the rounded tips of the *bowtie*, that could compromise the detection resolution of the resonance condition, making the optical characterization more difficult.

Low values of the resonance transmission are critical, because low values of input power $(P_{in} \sim 1 \text{ mW})$ are requested to avoid thermophoresis effect in the cavity, to preserve a stable trapping.

A decrease of the thickness of the silica layer induces an increase of Q/V with stronger light–matter interactions and high values of optical forces, but too low resonance transmission values.

The hybrid cavity performance for optical trapping has been also investigated with rounded tips of the *bowtie*, ranging the radius from 5 nm to 10 nm, to evaluate the effective influence of the pattern of the nanoantenna on the trapping efficiency. A decrease of optical forces has been observed with rounded tips, up to a maximum value of $F = -6$ pN and $F = -4$ pN with a radius of 5 nm and 10 nm, corresponding to $S = 60$ and $S = 40$, respectively, as shown in Table 3.

Similar performance also confirms the ability to trap nanoparticles with lower values of input power $(P_{in} \sim 1 \text{ mW})$ with rounded tips of the bowtie with a radius until 10 nm, providing $5 < S < 10$.

Those results demonstrate as the choice of $G = 150$ nm and $s = 50$ nm represents the best compromise between the hybrid cavity performance, in terms of the optical trapping stability, and the resolution detection.

5. Conclusion

We have designed a novel optical micro-resonator exhibiting very efficient vertical coupling between a 1-D PhC micro-cavity and a metal structure. The resonator has been accurately simulated and optimized using 3-D FEM techniques.

Due to the presence of a metal layer that generates narrow and very large field peaks, our hybrid plasmonic/photonic cavity exhibits a mode volume as small as $V = 4 \times 10^{-4}(\lambda/n)^3$. The Q-factor is 2.8×10^3 and the resonance transmission is $T = 47\%$ at $\lambda = 1589.62$ nm. The resulting Q/V ratio $(= 7 \times 10^6(\lambda/n)^{-3})$ improves the state-of-the-art of the hybrid devices with an integrated PhC cavity by a factor 100. The Q/V ratio is also comparable with that of PhC dielectric cavities. We have demonstrated that this result makes the proposed device very attractive for optical trapping.

We have evaluated an optical force $F = -26$ pN on a particle of 40 nm with an input power of 10 mW, confirming a high stiffness $K = 80$ pN/nm $\cdot$ W and a high stability $S = 210$ of the optical trap. A stability $S \geq 10$ has been also demonstrated for lower input power $(P_{in} < 1 \text{ mW})$, reducing the thermal heating effect and allowing longer detection time. The results confirm that the hybrid device is very suitable for trapping of single nanoparticle $(D < 100 \text{ nm})$, improving the performance achieved both by a single nanoantenna and a single PhC dielectric cavity.

References

[1] P. Velha *et al.*, "Ultra-High Q/V Fabry–Perot microcavity on SOI substrate," *Opt. Exp.*, vol. 15, no. 24, pp. 16 090–16 096, Nov. 2007.

[2] T. F. Krauss and R. M. De La Rue, "Photonic crystals in the optical regime—Past, present, and future," *Progress Quantum Electron.*, vol. 23, no. 2, pp. 51–96, Mar. 1999.

[3] R. De La Rue *et al.*, "Photonic crystal and photonic wire device structures," *Proc. SPIE*, vol. 5950, no. 595004, Oct. 2005.
[4] M. N. Armenise, C. E. Campanella, C. Ciminelli, F. Dell'Olio, and V. M. N. Passaro, "Phononic and photonic band gap structures: Modeling and applications," *Phys. Procedia*, vol. 3, no. 1, pp. 357–364, Jan. 2010.
[5] C. Ciminelli, F. Peluso, and M. N. Armenise, "Modeling and design of two-dimensional guided-wave photonic band-gap device," *J. Lightw. Tech.*, vol. 23, no. 2, pp. 886–901, Feb. 2005.
[6] C. Ciminelli, H. M. H. Chong, F. Peluso, R. M. De La Rue, and M. N. Armenise, "High-Q photonic crystal extended microcavity," in *Proc. ECOC*, Stockholm, Sweden, Sep. 2004, pp. 26–27, Post-deadline paper.
[7] C. Ciminelli and M. N. Armenise, "Modeling and design of a 2D photonic crystal microcavity on polymer material for sensing applications," in *Proc. SPIE 661933*, Jul. 2011, pp. 66 191–661 933.
[8] Q. Quan and M. Loncar, "Deterministic design of wavelength scale, ultra-high Q photonic crystal nanobeam cavities," *Opt. Exp.*, vol. 19, no. 19, pp. 18 529–18 542, Sep. 2011.
[9] H. Sekoguchi, Y. Takahashi, T. Asano, and S. Noda, "Photonic crystal nanocavity with a Q-factor of ~9 million," *Opt. Exp.*, vol. 22, no. 1, pp. 916–924, Jan. 2014.
[10] Y. Taguchi, Y. Takahashi, Y. Sato, T. Asano, and S. Noda, "Statistical studies of photonic heterostructure nano-cavities with an average Q factor of three million," *Opt. Exp.*, vol. 19, no. 12, pp. 11 916–11 921, Jun. 2011.
[11] J. S. Foresi *et al.*, "Photonic-bandgap microcavities in opticalwaveguides," *Nature*, vol. 390, pp. 143–145, Jul. 1997.
[12] R. M. De La Rue *et al.*, "Photonic crystal and photonic wire nano-photonics based on silicon-on-insulator," *New J. Phys.*, vol. 8, no. 256, Oct. 2006.
[13] P. Velha *et al.*, "Ultra-high Q/V Fabry–Perot microcavity on SOI substrate," *Opt. Exp.*, vol. 15, no. 24, pp. 16 090–16 096, Nov. 2007.
[14] B. Desiatov, I. Goykhman, and U. Levy, "Parabolic tapered photonic crystal cavity in silicon," *Appl. Phys. Lett.*, vol. 100, no. 4, pp. 041112, May 2012.
[15] J. D. Ryckman and S. M. Weiss, "Low mode volume slotted photonic crystal single nanobeam cavity," *Appl. Phys. Lett.*, vol. 101, no. 7, pp. 071104, Aug. 2012.
[16] A. M. Zain, N. P. Johnson, M. Sorel, and R. M. De La Rue, "Ultra high quality factor one dimensional photonic crystal/photonic wire micro-cavities in silicon-on-insulator (SOI)," *Opt. Exp.*, vol. 16, no. 16, pp. 12 084–12 089, Aug. 2008.
[17] H. C. Liu and A. Yariv, "Designing coupled-resonator optical waveguides based on high-Q tapered grating-defect resonators," *Opt. Exp.*, vol. 20, no. 8, pp. 9249–9263, Apr. 2012.
[18] P. Yu, B. Qi, X. Jiang, M. Wang, and J. Yang, "Ultrasmall-V high-Q photonic crystal nanobeam microcavities based on slot and hollow-core waveguides," *Opt. Lett.*, vol. 36, no. 8, pp. 1314–1316, Apr. 2011.
[19] Q. Quan, P. B. Deotare, and M. Loncar, "Photonic crystal nanobeam cavity strongly coupled to the feeding waveguide," *Appl. Phys. Lett.*, vol. 96, no. 20, pp. 203102, May 2010.
[20] K. J. Russel, T. Liu, S. Cui, and E. L. Hu, "Large spontaneous emission enhancement in plasmonic nanocavities," *Nature Photon.*, vol. 6, pp. 459–462, May 2012.
[21] H. Cho, C.O. Aspetti, J. Park, and R. Agarwal, "Silicon coupled with plasmon nanocavities generates bright visible hot luminescence," *Nature Photon.*, vol. 7, no. 4, pp. 285–289, Mar. 2013.
[22] K. J. Russell and E. L. Hu, "Gap-mode plasmonic nanocavity," *Appl. Phys. Lett.*, vol. 97, no. 16, pp. 163115, Oct. 2010.
[23] M. K. Kim *et al.*, "Low-loss surface-plasmonic nanobeam cavities," *Opt. Exp.*, vol. 18, no. 11, pp. 11 089–11 096, May 2010.
[24] X. Yang, A. Ishikawa, X. Yin, and X. Zhang, "Hybrid photonic-plasmonic crystal nanocavities," *ACS Nano*, vol. 5, no. 4, pp. 2831–2838, Apr. 2011.
[25] N. Descharmes, U. P. Dharanipathy, Z. Diao, M. Tonin, and R. Houdré, "Observation of backaction and self-induced trapping in a planar hollow photonic crystal cavity," *Phys. Rev. Lett.*, vol. 110, no. 12, pp. 123601, Mar. 2013.
[26] D. Erickson, X. Serey, Y. F. Chen, and S. Mandal, "Nanomanipulation using near field photonics," *Lab Chip*, vol. 11, no. 6, pp. 995–1009, Jan. 2011.
[27] T. van Leest and J. Caro, "Cavity-enhanced optical trapping of bacteria using a silicon photonic crystal," *Lab Chip*, vol. 13, no. 22, pp. 4358–4365, Aug. 2013.
[28] X. Serey, S. Mandal, Y. F. Chen, and D. Erickson, "DNA transport and delivery in thermal gradients near optofluidic resonators," *Phys. Rew. Lett.*, vol. 108, no. 4, pp. 048102, Jan. 2012.
[29] T. Franosch *et al.*, "Resonances arising from hydrodynamic memory in Brownian motion," *Nature*, vol. 478, no. 7367, pp. 85–88, Oct. 2011.
[30] W. Ding, R. Bachelot, S. Kostcheev, P. Royer, and R. E. De Lamaestre, "Surface plasmon resonances in silver Bowtie nanoantennas with varied bow angles," *J. Appl. Phys.*, vol. 108, no. 12, pp. 124314-1–124314-6, Dec. 2010.
[31] D. Conteduca, F. Dell'Olio, C. Ciminelli, T. F. Krauss, and M. N. Armenise, "Design of a new photonic/plasmonic microcavity allowing a strong light-matter interaction," in *Proc. 3rd Mediterranean Photon. Conf.*, Trani, Italy, May 7–9, 2014, pp. 1–3.
[32] I. H. Malitson, "Interspecimen comparison of the refractive index of fused silica," *J. Opt. Soc. Amer.*, vol. 55, no. 10, pp. 1205–1209, Oct. 1965.
[33] K. F. Palmer and D. Williams, "Optical properties of water in the near infrared," *J. Opt. Soc. Amer.*, vol. 64, no. 8, pp. 1107–1110, Aug. 1974.
[34] O. Painter *et al.*, "Two-dimensional photonic band-gap defect mode laser," *Science*, vol. 284, no. 5421, pp. 1819–1821, Jun. 1999.
[35] H. Fisher and O. J. F. Martin, "Engineering the optical response of plasmonic nanoantennas," *Opt. Exp.*, vol. 16, no. 12, pp. 9144–9154, Jun. 2008.
[36] A. D. Rakic, A. B. Djurisic, J. M. Elazar, and M. L. Majewski, "Optical properties of metallic films for vertical-cavity optoelectronic devices," *Appl. Opt.*, vol. 37, no. 22, pp. 5271–5283, Aug. 1998.
[37] M. Ploshner, M. Mazilu, T. F. Krauss, and K. Dholakia, "Optical forces near a nanoantenna," *J. Nanophoton.*, vol. 4, no. 1, pp. 041570-1–041570-13, Jan. 2010.

[38] S. Lin, J. Hu, L. Kimerling, and K. Crozier, "Design of nanoslotted photonic crystal waveguide cavities for single nanoparticle trapping," *Opt. Lett.*, vol. 34, no. 21, pp. 3451–3453, Jun. 2009.
[39] K. Dholakia and T. Cizmar, "Shaping the future of manipulation," *Nature Photon.*, vol. 5, no. 6, pp. 335–342, May 2011.
[40] Y. Pang and R. Gordon, "Optical trapping of a single protein," *Nano Lett.*, vol. 12, no. 1, pp. 402–406, Jan. 2012.
[41] O. Brzobohaty *et al.*, "Experimental demonstration of optical transport, sorting and self-arrangement using a tractor beam," *Nature Photon.*, vol. 7, no. 2, pp. 123–127, Jan. 2013.
[42] B. J. Roxworthy *et al.*, "Application of plasmonic bowtie nanoantenna arrays for optical trapping, stacking, and sorting," *Nano Lett.*, vol. 12, no. 2, pp. 796–801, Feb. 2012.
[43] T. Tlusty, A. Meller, and R. B. Ziv, "Optical gradient forces of strongly localized fields," *Phys. Rev. Lett.*, vol. 81, no. 8, pp. 1738–1741, Aug. 1998.
[44] Y. F. Chen, X. Serey, R. Sarkar, P. Chen, and D. Erickson, "Controlled photonic manipulation of proteins and other nanomaterials," *Nano Lett.*, vol. 12, no. 3, pp. 1633–1637, Mar. 2012.
[45] A. H. J. Yang and D. Erickson, "Optofluidic ring resonator switch for optical particle transport," *Lab Chip*, vol. 10, no. 6, pp. 769–774, Mar. 2010.
[46] J. Wu and X. Gan, "Three dimensional nanoparticle trapping enhanced by surface plasmon resonance," *Opt. Exp.*, vol. 18, no. 16, pp. 27 619–27 626, Dec. 2010.
[47] Y. Pang and R. Gordon, "Optical trapping of 12 nm dielectric spheres using double-nanoholes in a gold film," *Nano Lett.*, vol. 11, no. 9, pp. 3763–3767, Aug. 2011.
[48] X. Serey, S. Mandal, and D. Erickson, "Comparison of silicon photonic crystal resonator designs for optical trapping of nanomaterials," *Nanotech.*, vol. 21, no. 30, pp. 305202, Jul. 2010.
[49] A. H. J. Yang and D. Erickson, "Stability analysis of optofluidic transport on solid-core waveguiding structures," *Nanotechnol.*, vol. 19, no. 4, pp. 045704, Jan. 2008.